ARTICLE OPEN

Check for updates

Partial truncation of the C-terminal domain of PTCH1 in cancer promotes tumourigenesis by non-canonical activation of a GLI-PI3K loop

Begoña Caballero-Ruiz[1,2], Rosa Bordone[1], Sonia Coni[1], Danai S. Gkotsi[2], Eva Gonzalez[2], Gianluca Canettieri[1,3]✉ and Natalia A. Riobo-Del Galdo[2,4]✉

Loss of function mutations of the Hedgehog receptor PTCH1 are oncogenic drivers in some skin and brain cancers. We recently reported mutations in exons encoding the C-terminal tail of PTCH1 in colon cancer, which result in premature truncation but do not impair canonical Hedgehog signalling. In this study, we show that colon cancer cells engineered by CRISPR/Cas9 to express endogenous truncated PTCH1 have enhanced proliferation, colony formation, anchorage-independent growth and form larger tumours in vivo than isogenic cells expressing wild-type PTCH1. Analysis of the mechanisms underlying this growth advantage revealed profound transcriptional changes and unexpectedly, upregulation of GLI1 and GLI2 by a Smoothened-independent route, which proved to be necessary for the proliferative advantage. Furthermore, we found that truncation of PTCH1 C-tail upregulated several cancer-related pathways, including EGFR and Ras signalling and led to enhanced GLI-dependent PI3K activation, which exerted a positive feedback regulation on GLI expression and activity. Accordingly, PTCH1 mutant cells were highly sensitive to PI3K and GLI inhibitors and were only partially sensitive to EGFR and MEK inhibitors. Altogether, these findings reveal that PTCH1 C-tail truncating mutations promote colon cancer tumourigenesis through a non-canonical GLI-PI3K positive loop.

Oncogene (2026) 45:1013–1025; https://doi.org/10.1038/s41388-026-03698-9

INTRODUCTION

The Hedgehog (Hh) pathway plays an essential role in embryonic development, tissue regeneration, cell fate and stem cell renewal [1–3]. Canonical Hh signalling is triggered by binding of one of the three Hh ligands (Sonic, SHH; Indian, IHH; or Desert, DHH) to the receptor Patched1 (PTCH1), leading to derepression of Smoothened (SMO) and activation of the GLI-family of transcription factors. The presence of Hh ligands is sensed by the constitutively expressed GLI2 and GLI3 isoforms, which then induce expression of GLI1, PTCH1, and other cell type-specific genes [3]. Hh binding to PTCH1 also inhibits non-canonical PTCH1 intrinsic functions that are independent of SMO/GLI signalling, such as proapoptotic signalling and inhibition of autophagy [4–6]. These functions of PTCH1 are mediated by its C-terminal domain (CTD), a 273 amino acids-long intrinsically disordered region that acts as a protein-protein interaction hub for ubiquitin E3 ligases, DRAL/TUCAN-1/procaspase-9, and ATG101 [5, 7, 8]. However, most of the CTD is dispensable for canonical Hh signalling via SMO and GLI transcription factors [9, 10].

Excessive activation of canonical Hh signalling is common in many cancers, with loss-of-function mutations in *PTCH1* and gain-of-function mutations in *SMO* driving tumourigenesis in a Hh ligand-independent manner in most basal cell carcinomas of the skin and the SHH-type medulloblastoma [11]. Upregulation of SHH and IHH without pathway mutations is a common finding in carcinomas and adenocarcinomas from the GI tract [12–14]. In addition, multiple oncogenic pathways can lead to activation or potentiation of GLI transcriptional activity. Indeed, there is increasing evidence that regulation of GLI proteins in cancer might also occur through non-canonical signalling pathways, reducing therapeutic efficacy of SMO antagonists [15].

In a previous study we reported that indel mutations in exons 22-23 encoding the CTD of PTCH1 in 5-13% human colon, stomach, and endometrial cancers result in loss of PTCH1 interaction with ATG101 [16]. The mutational hotspots S1203fs, R1308fs and Y1316fs, enriched in right-sided MSI+ colon cancer, result in premature stop codons. We reported that these frameshift mutations lead to loss of interaction with ATG101, increasing both basal and induced autophagy, and promote survival under nutritional stress [16]. Based on those findings, we hypothesised that partial truncation of PTCH1 reduces its tumour suppressor activity. In this study, we demonstrate that homozygous CTD truncation of endogenous PTCH1 in colon cancer cells engineered by CRISPR/Cas9 have a proliferative advantage in vitro and in vivo compared to isogenic cells expressing wild type PTCH1. The increased fitness is provided by a SMO-independent, PI3K-dependent upregulation of GLI1 and other profound transcriptome changes. In summary, we report

[1]Department of Molecular Medicine, Sapienza University of Rome, Rome, Italy. [2]School of Molecular and Cellular Biology, Faculty of Biological Sciences, University of Leeds, Leeds, UK. [3]Institute Pasteur Italy-Cenci Bolognetti Foundation, Rome, Italy. [4]Astbury Centre for Structural Molecular Biology, University of Leeds, Leeds, UK.
✉email: Gianluca.canettieri@uniroma1.it; n.a.riobo-delgaldo@leeds.ac.uk

Received: 11 June 2025 Revised: 14 January 2026 Accepted: 6 February 2026
Published online: 26 February 2026

for the first time that PTCH1 CTD truncations found in cancer underlie a more aggressive phenotype in vivo and in vitro in a manner that is insensitive to SMO inhibitors but sensitive to PI3K inhibitors.

MATERIAL AND METHODS

Cell lines and cultures

Scrambled (SCR) and PTCH1 CTD mutant SW620 cells (C9 and C15) were previously described [16]. LoVo (CCL-229) and SW480 (CCL-228) were purchased from ATCC (Manassas, VA, USA). *Ptch1*$^{-/-}$ mouse embryonic fibroblasts were a gift from Dr. Matthew Scott (Stanford University). All cell lines were maintained in Dulbecco's modified Eagle medium (DMEM, high glucose, Sigma-Aldrich) supplemented with 10% Foetal Bovine Serum (FBS) (GIBCO), 1 mM penicillin-streptomycin (Sigma-Aldrich) and 1 mM glutamine (Sigma-Aldrich) in a humidified incubator at 37 °C and 5% CO_2.

Treatment with inhibitors

Cells were exposed to KAAD-Cyclopamine (Biovision #1910-50), Erlotinib (Selleckchem #S7786), Cetuximab (C225) (TargetMol #T9905), GANT61 (Stratech Scientific Ltd #A1615), SD208 (Selleckchem #S7624), Trametinib (Selleckchem #S2673), UO-126 (Selleckchem #S1102), BKM120 (Selleckchem #S2247), or LY294002 (Thermo Fisher #PHZ1144) dissolved in DMSO. Treatments were performed in complete growth medium for the indicated time and concentration.

Animal studies

For the xenograft studies, animals ($n = 6$ per experimental group) were randomly assigned to receive subcutaneous injections of 2×10^6 SCR cells (SCR group) or C9 cells (C9 group). Tumor cells were resuspended in 70 µl phosphate-buffered saline (PBS) and mixed 1:1 with Matrigel (Corning, #354248) before implantation into both flanks of 5-week-old female athymic nude mice (CD1, Charles River Laboratories). Once tumors reached a volume of 100 mm^3, their size was measured every 3 days using a caliper without blinding. Animals were euthanized after 3 weeks, and all tumor masses were excised. The experiment was independently repeated twice.

Data are presented as mean ± standard deviation for each experimental group and time point. For each time point, a two-tailed Student's t-test was used to compare groups, and p-values < 0.05 and < 0.01 were considered statistically significant and are indicated as * and **, respectively. Sample size was determined a priori using G*Power software.

All animal procedures complied with the European Community Council Directive 2010/63/EU and were approved by the local Ethical Committee for Animal Experiments of Sapienza University of Rome (Authorization no. 877/2016-PR).

Immunohistochemistry

Freshly excised xenografts were fixed in 4% paraformaldehyde for 24 h at 4°C, paraffin embedded and sectioned at 5 µm using a RM2245 microtome (Leica Biosystems, Wetzlar, Germany). Antigen was retrieved using 1X Tris-EDTA, pH 9.0 (Himedia #ML087). Sections were incubated with Gli1 (Cell Signaling Technology # 2643S) and Ki67 (Pierce #MA5-14520) antibodies followed by biotinylated goat anti-polyvalent secondary antibody and streptavidin-conjugated horseradish peroxidase and visualised with DAB using the Mouse-to-Mouse Kit (ScyTek Laboratories #MTM001). Images were captured using a ZEISS Axiocam 208 colour (ZEISS Group, Oberkochen, Germany) on a ZEISS Axiolab 5 light microscope (ZEISS Group).

Colony formation assays

Cells (1×10^3 cells/well) were seeded into 6-well plates in complete DMEM and 24 h later treated with inhibitors or DMSO. After 10 days, cells were fixed with 100% methanol, stained with 0.005% crystal violet (Sigma-Aldrich #V5265), and colonies were counted.

Soft agar colony formation assay

A cell suspension containing 5×10^3 cells was added to each well of a 6-well plate in soft agar (ThermoScientific #R0801) as previously described [17]. Once the colonies were visible (typically after 15 days), colonies were stained with 0.005% crystal violet solution for counting.

Proliferation assay

Cells (4×10^4/well) were seeded in 24-well plates and incubated overnight at 37 °C. After 24 h, cells were trypsinised and live cells were counted (time = 0) by the trypan blue exclusion method. Cells were then treated with the different inhibitors at the concentrations indicated in the text. Every 24 h cells were trypsinised and counted following the same method.

For WST-1 proliferation assay, 2×10^3 cells/well were seeded in 96-well plate in 100 µl and left for 24 h before being subjected to different treatments. At each time point, 10 µl of WST-1 reagent (Roche Applied Sciences #05015944001) was added to each well and incubated for 0.5- 4 h at 37 °C, 5% CO_2. Then, the plate was shaken for 1 min and absorbance measured using a microplate reader at 420–480 nm.

EdU incorporation assay

The Click-iT EdU Alexa Fluor 488 HCS Assay (Invitrogen, #C10350) was performed following the manufacturer's protocol to assess cell proliferation. Specifically, cells were supplemented with EdU for 6 h prior to fixation with 3.7% formaldehyde in phosphate-buffered saline (PBS). Permeabilization was achieved using 0.5% Triton X-100 in PBS. The Click-iT reaction cocktail was prepared as specified by the manufacturer and incubated for 30 min. Finally, nuclei were counterstained by adding 1X Hoechst 33342 solution for 10 min. Confocal images were acquired using a ZEISS LSM 980 with Airyscan 2 laser-scanning confocal microscope, employing a 63× Oil immersion objective to count the percentage of EdU+ nuclei.

Transient transfections

For transfection assays, cells (8×10^4 /well) were seeded in a 12-well plate. On the following day, cells were transfected with Lipofectamine 2000 (Thermo Fisher #11668019) using 1.5 µl transfection reagent and 0.38 µg of DNA in Opti-MEM medium (Thermo Fisher # 31985-062). Before transfection, cells were washed once with PBS and the culture medium was replaced with Opti-MEM. The lipid-DNA complexes were then added to the cells. Cells were incubated with the transfection mixture for 6 h at 37 °C. Then, the media was replaced with complete growth medium lacking antibiotics. The following day, medium containing antibiotics was added to the cells. At the indicated time points, cells were trypsinised, counted following the trypan blue exclusion method and lysed for protein analysis. The plasmids encoding Akt1 (T308A and S473A) and myr-Akt1 were gifts of J. Testa (Fox Chase Cancer Center, Philadelphia). PKA-CQR was a gift from S. McKnight (University of Washington, Seattle). pcDNA3.1+ (Invitrogen) was used as empty control plasmid.

For transfections with Gli1 K518R and Gli1(2-413)-VP16 [18] cells (2×10^5/cm^2) were seeded in 21-cm^2 culture dishes and transfected following the method previously described. After 48 h from transfection, cells were then detached and a small aliquot was collected and processed for Western blot analysis to assess mutant overexpression, while the remaining cells were reseeded at 2×10^4/well in 24-well plate. Cell number was quantified 72 h later using trypan blue exclusion method.

Western blotting

Cells or tissues were lysed in denaturing buffer containing 50 mM Tris-HCl, 2% SDS, 10% Glycerol, 10 mM $Na_4P_2O_7$, 100 mM NaF, 6 M Urea, 10 mM EDTA or by direct lysis in RIPA buffer (Thermo Scientific # 89900) containing protease and phosphatase inhibitor cocktails for western blotting (Thermo Scientific #87785 # 78420). Protein extracts were quantified with the Pierce BCA protein assay kit (ThermoScientific # 23227) and resolved by SDS-PAGE. Separated proteins were transferred to a nitrocellulose (Perkin Elmer # NBA085C001EA) or PVDF membrane (BioRad #1620177), blocked in 5% non-fat dried milk in Tris-buffered saline with 0.05% Tween 20 (TBST) (Sigma #P7949), and incubated overnight with primary antibodies at 4°C at the specified concentrations. Next day, membranes were washed in TBST and incubated with HRP-conjugated secondary antibodies at RT for 1 h and developed using WesternBright ECL (Advansta #K-12045-D50) in a ChemiDoc imaging system (BioRad) using the Image Lab software (BioRad). Signal intensity was quantified by ImageJ software and normalized to loading control indicated in the text.

Antibodies

The following antibodies were used: EGFR (Cell Signaling Technology #2256, WB 1:1,000), AKT (Cell Signaling Technology #4691, WB 1:1,000), phospho- AKT (Ser473) (D9E) XP (Cell Signaling Technology #5012, WB 1:1,000), p44/42 MAPK (Erk1/2) (Thr202/Tyr204) (Cell Signaling Technology #4695, WB 1:1,000), phospho-p44/42 MAPK (Erk1/2) (Thr202/Tyr204) (Cell

Signaling Technology #4376, WB 1:1,000), Gli1 (Cell Signaling Technology #2643, WB 1:1,000), Phospho-PKA substrate (Cell Signaling Technology #9624, WB 1:1,000), GAPDH-HRP (Proteintech #HRP-60004, WB 1:3,000), Vinculin (Santa Cruz #sc-73614, WB 1:10,000), Poly-ADP ribose Polymerase (Cell Signaling Technology #9542, WB 1:2,000), anti VP16 (Santa Cruz #sc7545, WB 1:1,000),HA-Tag (Invitrogen #26183, WB 1:10,000), goat anti-rabbit IgG HRP (BioRad #172-1019, WB 1:3,000), goat anti-mouse IgG (H L)-HRP conjugate (Bethyl #A90-116P, WB 1:3,000).

Quantitative Real-Time PCR (qPCR) assay

Total mRNA was isolated with RNeasy Mini Kit (QI-AGEN #74104) or by Trizol method. Synthesis of cDNA was performed using 1 µg RNA with the Sensifast cDNA synthesis kit (Bioline #BIO-65054) or iScript cDNA Synthesis Kit (BioRad #1708897) using hexa-random primers. Real-time quantitative PCR was performed using 2 µL of cDNA and target-specific primers (Table S1) and the SsoFast EvaGreen Supermix (BioRad #1725201) or SensiFast Sybr Lo-Rox Mix (Bioline #BIO-94020) in a CFX Connect Real-Time PCR System (BioRad) or ViiA 7 Real-Time PCR System (Applied Biosystems). Amplification was quantified using the ΔΔCt method, where ΔCt is the difference of the Ct value between the target gene minus the Ct value of the control gene (GAPDH), and the second Δ is the difference between a PTCH1 CTD mutant clone and the SCR control.

RNAseq library construction, quality control and sequencing

Total RNA from the 3 cell clones in three consecutive cell passages was isolated with RNeasy Mini Kit (QIAGEN #74104). After fragmentation, cDNA was synthesised using hexa-random primers, followed by adaptor ligation, size selection, amplification and purification. The library was checked with Qubit and real-time PCR for quantification and bioanalyzer for size distribution detection. Quantified libraries were sequenced on Illumina PE150 platforms to generate paired-end reads at Novogene.

RNA-seq data analysis

Raw data in fastq format were cleaned using fastp software, aligned to the GRCh38 human reference genome using Hisat2 v2.0.5., the number of reads mapped to each gene quantified with featureCounts v1.5.0-p3, followed by calculation of FPKM (Fragments Per Kilobase of transcript sequence per Millions base pairs sequenced) per gene. Differential expression analysis was performed using the DESeq2 R package (1.20.0). The resulting P-values were adjusted using the Benjamini and Hochberg's approach for controlling the false discovery rate (FDR). Genes with an adjusted P-value <=0.05 found by DESeq2 were assigned as differentially expressed.

Enrichment analysis of differentially expressed genes

Gene Ontology (GO) enrichment analysis of differentially expressed genes (DEG) was implemented by the clusterProfiler R package. GO terms with corrected P-value < 0.05 were considered significantly enriched. We tested the statistical enrichment of DEGs in KEGG, Reactome, Disease Ontology (DO) and DisGeNET pathways databases using clusterProfiler R package, with a $P < 0.05$ cutoff.

Gene set enrichment analysis (GSEA)

The DEGs between the 3 cell lines were ranked according to the degree of differential expression and the P-value. They were compared to predefined Gene Sets to determine if they were enriched at the top or bottom of the list using a local version of the GSEA analysis tool (http://www.broadinstitute.org/gsea/index.jsp).

Lentiviral-mediated shRNA knockdown

shRNA knockdown of GLI1 was performed through lentiviral infection. Lentiviruses were generated in HEK293 cells transfected with pLKO.1 vectors encoding shGLI1 (sh-hGLI1-85: 5′ CCGGCCTGATTATCTTCCTTCA-GAATCTAGATTCTGAAGGAAGATAATCAGGTTTTTG, and sh-hGLI1-87: 5′ CCGGCCAAACGCTATACAGATCCTATCTAGATAGGATCTGTATAGCGTTTG GTTTTTG) or a scrambled sequence together with 15 µg of pCMV-R 8.74, and 10 µg of pMDG with the calcium phosphate method. After 24 h, the medium was changed and then collected at 48 h and stored at −80 °C. Control shRNA (scrambled, #SHC002) was obtained by Sigma-Aldrich. Viral titers were determined by qPCR as previously described [19]. For lentiviral transduction, 4×10^5 cells were seeded overnight in 60 mm dishes. The day after, 1 ml of a 1:1 Sh-Gli1-85 and 87 virus-containing media was added to cells with 5 µg/ml polybrene (Sigma-Aldrich #H9268) and cells were incubated for 72 h. Knockdown efficiency was monitored by western blotting and qPCR.

Statistical analysis

Statistical analysis and generation of graphs was performed using GraphPad Prism 9 (GraphPad Software, La Jolla, California, USA, https://www.graphpad.com/). Data were analyzed by Student's t-test to analyse the significant difference between two groups. One-way ANOVA analysis was selected to analyse at least three different groups when the samples showed normal distribution and equal variance, followed by post-hoc Tukey's test for multiple comparisons. Figure legends indicate statistical details of experiments.

RESULTS

PTCH1 CTD truncation enhances tumourigenesis in vitro and in vivo

To investigate the biological consequences of cancer-associated PTCH1 frameshift mutations that result in premature truncation of the CTD in the 1203-1316 region, we engineered indel mutations at position D1222 of PTCH1 in the colon cancer cell line SW620 by CRISPR/Cas9 (Fig. S1A). SW620 cells contain mutations in *KRAS* and *TP53* (homozygous *RAS(G12V);* heterozygous *TP53(R273H)/TP53(P309S)*) [20]. We selected two single-cell derived clones harbouring different frameshift-causing mutations (C9 and C15) alongside the parental cells containing wild-type PTCH1 (SCR) to lower the risk of picking up a non-specific phenotype (Fig. S1B, C) [16, 21]. To investigate phenotypic changes caused by PTCH1 CTD truncation, we first examined the proliferative capacity of the C9 and C15 cells in vitro. Both PTCH1 mutant clones exhibited accelerated growth, reflected as an increase in cell number of ~2-fold over the parental SCR cells after 96 h (Fig. 1A). C9 and C15 cells exhibited increased proliferation, as determined by Edu incorporation (Fig. 1B) and reduced apoptosis, assessed by cleavage of Poly-ADP ribose polymerase (PARP) (Fig. 1C). In agreement, C9 and C15 cells showed a much higher colony forming capacity than SCR cells, with an average 13.3-fold (C9, $p < 0.001$) and 11-fold (C15, $p < 0.01$) increase (Fig. 1D). We also evaluated the anchorage-independent growth of the cells in soft agar, reflecting resistance to anoikis. The number of anchorage-independent colonies formed by C9 and C15 cells was increased by 8-fold ($p < 0.0001$) and 4-fold ($p < 0.0001$), respectively, compared to SCR cells (Fig. 1E). Therefore, SW620 cancer cells with PTCH1 CTD truncations have a much higher proliferative and survival capacity in vitro irrespective of their surrounding environment. Importantly, C9 and C15 cells expressed similar or greater levels of *PTCH1* at the transcript level, ruling out nonsense-mediated decay (Fig. S1D). Therefore, the phenotype of PTCH1 CTD mutant cells is unlikely to be caused by functional PTCH1 deficiency.

Next, we grafted SCR or C9 cells into the flanks of athymic nude mice to evaluate the effect of PTCH1 CTD truncations on tumour growth in vivo over 21 days. C9 cells xenografts grew significantly faster compared to SCR control tumours. The growth advantage of C9 cells was evident from day 6 onwards, showing a 183% increase in tumour volume ($p < 0.05$) and a 211% increase in weight ($p < 0.001$) compared to tumours formed by SCR parental cells at day 21 (Fig. 1F, G). Consistently, Ki67 staining was increased in C9 tumours compared to SCR xenografts (Fig. 1H).

The results of altered oncogenic properties of isogenic colorectal cancer cells that differ in the mutational status of the PTCH1 CTD in vitro and in vivo strongly indicates that partial truncation of the PTCH1 CTD confers a growth advantage and a more malignant phenotype.

Non-canonical activation of the GLI transcription factors mediates the growth advantage of cancer cells with truncation in the PTCH1 CTD

We next set to investigate the mechanism by which truncation of the PTCH1 CTD provides an oncogenic advantage. We first investigated if truncation of the PTCH1 CTD results in activation of canonical Hh signalling. We tested this using *Ptch1*$^{-/-}$ mouse embryonic fibroblasts, in which loss of Ptch1 results in constitutive activation of SMO and high Gli-transcriptional activity (Fig. S2A). In agreement with previous work [9], introduction of PTCH1 CTD truncation mutants lacking increasingly longer regions of the CTD have comparable activity to wild-type PTCH1 to inhibit basal Gli-luciferase activity in *Ptch1*$^{-/-}$ MEFs (Fig. S2B). In addition, point mutations and small deletions in the CTD regions 1195-1998 and 1216-1235 do not affect canonical Hh signalling (H. Ollerton, F. Cross, NA Riobo-Del Galdo, unpublished data). Combined with the absence of nonsense-mediated decay of the mutant PTCH1 transcripts, this suggests that the cancer-associated truncations of the CTD do not promote oncogenic properties by derepression of SMO. To confirm this, we determined the expression level of *GLI1*, a GLI-target gene used as a hallmark of canonical Hh signalling. Unexpectedly, both C9 and C15 cells showed a strong expression of GLI1 at the protein level compared to SCR control cells (Fig. 2A). Furthermore, not only *GLI1* but also *GLI2*, a constitutively expressed mediator of canonical Hh signalling, were transcriptionally upregulated between 6 and 9-fold in C9 and C15 cells (Fig. 2A). In agreement with the findings in cultured cells, C9-derived tumours xenograft masses showed strong GLI1 signal by immunohistochemistry compared to SCR-derived tumours (Fig. 2B).

Given the unexpected upregulation of GLI1 in PTCH1 CTD mutant cells, we performed a series of experiments to determine if increased GLI signalling was implicated in their augmented oncogenic properties. Treatment of the cell lines with the dual GLI1/GLI2 inhibitor GANT61 blocked proliferation in SCR, C9 and C15 cells in a dose-dependent manner, although C9 and C15 cells were more sensitive to lower concentrations of GANT61 (Figs. 2C and S3). Importantly, the SMO inhibitor KAAD-cyclopamine did not affect cell viability of any of the cell lines, while GANT61 had a strong inhibitory effect (Figs. 2D and S3), which ruled out the possibility that GLI1 upregulation in PTCH1 CTD cells is caused by activation of canonical Hh signalling. In addition, GANT61 dramatically reduced colony formation of C9 and C15 clones to the level of SCR cells (Fig. 2E, F). To confirm the specific effect of GANT61, we stably knocked down GLI1 expression using an shGLI1-encoding lentivirus, while using a scrambled shScr as control (Fig. 2G). In agreement with the cytotoxic effect of GANT61, silencing of GLI1 reduced viability in C9 and C15 cells but not in SCR cells (Fig. 2H), suggesting that GLI1 upregulation is essential for the growth advantage imparted by truncation of the PTCH1 CTD. Next, we tested whether expression of a constitutively active form of GLI1 in SCR cells was sufficient to impart a proliferative advantage. Two different active GLI1 mutants were transiently transfected into SCR cells: an acetylation-deficient mutant (GLI1 K518R) and a Gli1-VP16 fusion protein which render GLI1 constitutively active [18]. Both active GLI1 mutants increased proliferation of SCR cells to a similar level of C9 and C15 cells (Fig. 2I. Expression of the plasmids was verified by Western blot analysis (Fig. 2J). These results suggest that GLI1 upregulation in CTD mutant clones is exclusively through non-canonical pathways independent of SMO, and that GLI upregulation is essential for their more aggressive cancer behaviour. Finally, we investigated if colon cancer cell lines that naturally acquired a PTCH1 CTD truncation are highly dependent on GLI1, like the CRISPR/Cas9 engineered C9 and C15 clones. Screening of the Cancer Cell Line Encyclopedia database (Broad Institute) identified indel mutations in the PTCH1 CTD in LoVo and SW480 cells. Culture of both cell lines in the presence of low GANT61 concentrations (5 μM) strongly reduced cell numbers over time (Fig. 3A, C). Stable knockdown of GLI1 using a lenti-shGLI1 vector also abolished cell proliferation in LoVo and SW480 cells (Fig. 3B, D). Altogether, these data indicate that mutations that lead to partial truncation of PTCH1 CTD confer a proliferative advantage through a non-canonical upregulation of GLI1.

Truncation of the PTCH1 CTD induces vast transcriptome changes and upregulation of multiple oncogenic pathways

To explore the mechanisms underlying the oncogenic role of PTCH1 CTD mutations, we performed transcriptome analysis in C15, C9 cells and parental cells (SCR). RNA-seq was performed in each cell line on three consecutive passages to obtain meaningful biological repeats. Data analysis revealed a significant overlap of a set of genes only expressed in C9 and C15 cells (1396 genes) but not in SCR cells (Fig. 4A), while each clone had ~400 unique genes that were not considered for further analysis. Pearson correlation analysis confirmed the similarity between C9 and C15, with the largest differences observed between C9 and SCR cells (Fig. 4B). Therefore, pooled read counts from C9 and C15 (renamed as "PTCH1 mut" group) was compared to SCR cells (renamed "WT") to identify genes and pathways dysregulated in cells with PTCH1 CTD truncations, revealing upregulation of 3,619 genes and downregulation of 1,705 genes (Fig. 4C and Tables S2 and S3). Comparison of C9 vs. C15 transcriptomes showed differential expression of only 111 genes (Fig. S4 and Table S4), indicating a very similar transcriptome in C9 and C15 cells, despite carrying different PTCH1 CTD indels, and a divergence of the isogenic WT cells.

KEGG pathway enrichment analysis of the differentially expressed genes (DEGs) between PTCH1 mut vs. WT cells showed increase in gene signatures of cancer-related pathways, including *MAPK signalling pathway*, *cAMP signalling pathway, Ras signalling pathway*, and *Basal Cell Carcinoma* (Fig. 4D). Gene set enrichment analysis (GSEA) of ranked gene lists also revealed enrichment of general pathways in cancer, including Ras, MAPK, HIF1 and basal cell carcinoma, as well as pathways regulating pluripotency, cAMP and calcium signalling (Fig. S5).

Table 1 shows selected upregulated genes in both C9 and C15 clones involved in key pathways in tumourigenesis by RNA-seq. In agreement with the increased level of GLI1 in C9 and C15 cells, RNA-seq revealed increased *GLI1* and *GLI2* levels as well as some key GLI target genes (*HHIP* and *PTCH2*); however, no change in Hh ligands or *SMO* were observed and the negative regulator *GLI3* was downregulated 19-fold (Table S3). Amongst the most upregulated genes were genes belonging to the epidermal growth factor receptor (EGFR) signalling pathway: *EGFR* and several of its ligands, components of the TGFβ signalling pathway and regulators of cAMP-dependent kinase signalling (Table 1). These transcriptomic changes suggest that multiple pathways could mediate the non-canonical upregulation of GLI1 and GLI2 by activation of GLI positive modulators and/or inhibition of negative regulators. For instance, cAMP-dependent kinase (PKA) is the main negative regulator of all GLI proteins. It phosphorylates all GLI isoforms, targeting GLI1 for proteasomal degradation and GLI2 and GLI3 for processing into transcriptional repressors [1]. The upregulation of several cAMP phosphodiesterases in PTCH1 mutant cells led us to examine cAMP and PKA activity level. As suggested by the RNA-seq changes, PTCH1 CTD mutant cells produced much lower cAMP in response to forskolin (~65–80% of SCR cells) (Fig. 4E), suggesting a reduced PKA activity. Phosphorylation of PKA substrates, containing the RRX(S/T) motif, was diminished in C9 and C15 cells compared to SCR cells (Fig. 4F). Based on this, we hypothesised that reduced PKA activity mediates their proliferative advantage through activation of GLI-dependent signalling. Transfection of a constitutively active PKA α subunit (PKA-CQR) increased phosphorylation of PKA substrates (Fig. 4F) and specifically reduced proliferation of C9 and C15 cells

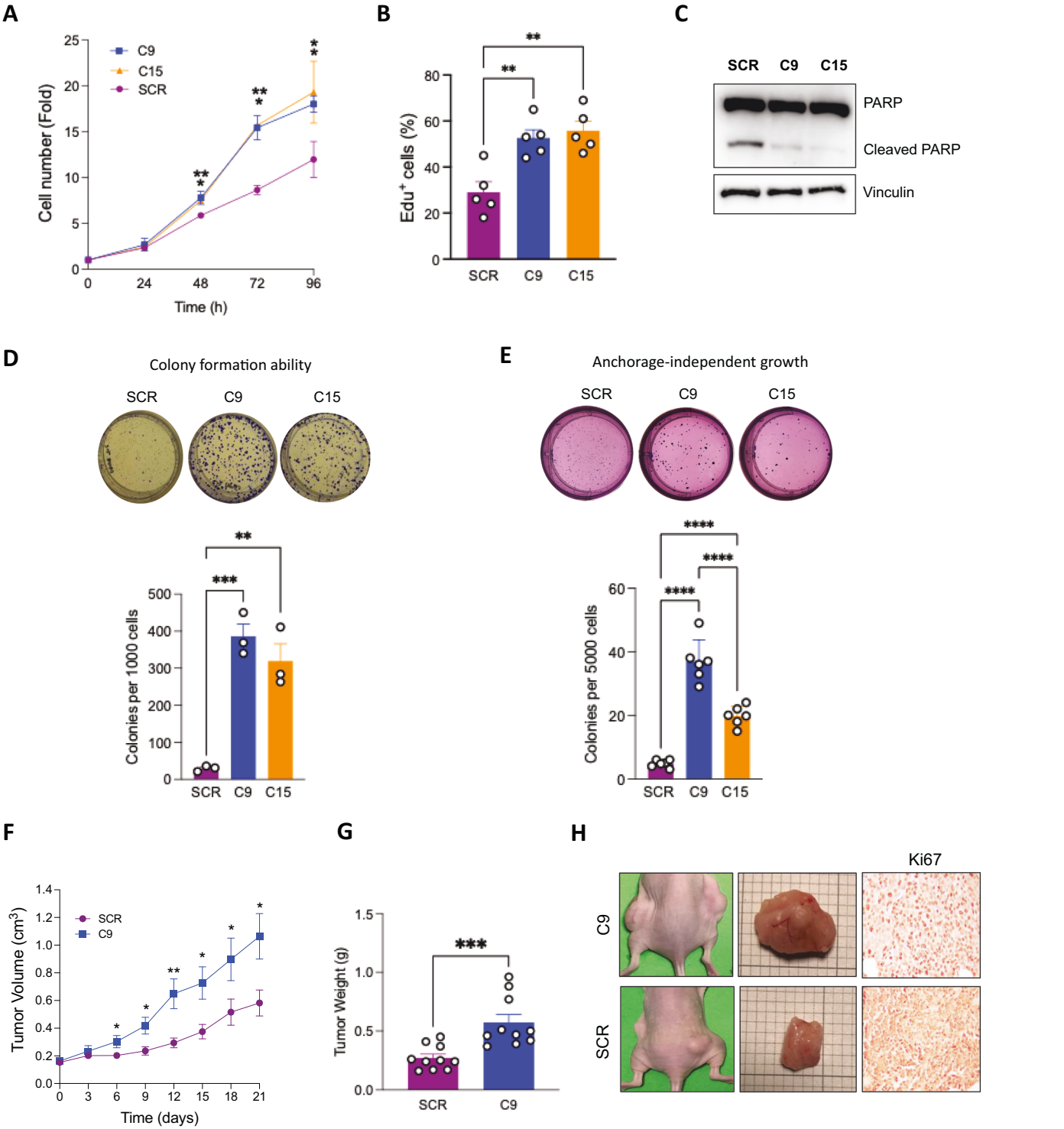

Fig. 1 Isogenic colon cancer cells with PTCH1 CTD truncation have a proliferative advantage in vitro and in vivo. A Change in cell number of SCR, C9 and C15 cells over time in complete medium ($n = 3$). **B** EdU incorporation, quantified as % of total nuclei, in SCR, C9 and C15 over time in complete medium ($n = 3$). **C** Representative immunoblot of full-length PARP and cleaved PARP in SCR, C9 and C15 cells. Expression of vinculin was used a a loading control. **D** Colony formation ability of SCR, C9 and C15 during 10 days of culture. Top. Representative images at the end of the experiment. Bottom: number of colonies per 1000 cells plated at day 10 ($n = 3$). **E** Anchorage-independent growth of SCR, C9 and C15 cultured in soft agar for 15 days. Top: representative images at the end of the experiment. Bottom: number of colonies per 5000 cells plated at day 15 ($n = 6$). **F** Changes in tumour volume over time of xenograft tumours after injection of SCR or C9 cells in the flanks of nude mice. **G** Weight of xenografts from SCR or C9 cells at the end of the experiment ($n = 10$). **H** Representative images of xenograft mice and isolated tumours at the end of the experiment. Representative images for IHC staining of Ki67 in sections of xenograft masses. All quantitative data represent the mean ± SEM of independent biological repeats. *$P < 0.05$; **$P < 0.01$; ***$P < 0.001$; ****$P < 0.0001$.

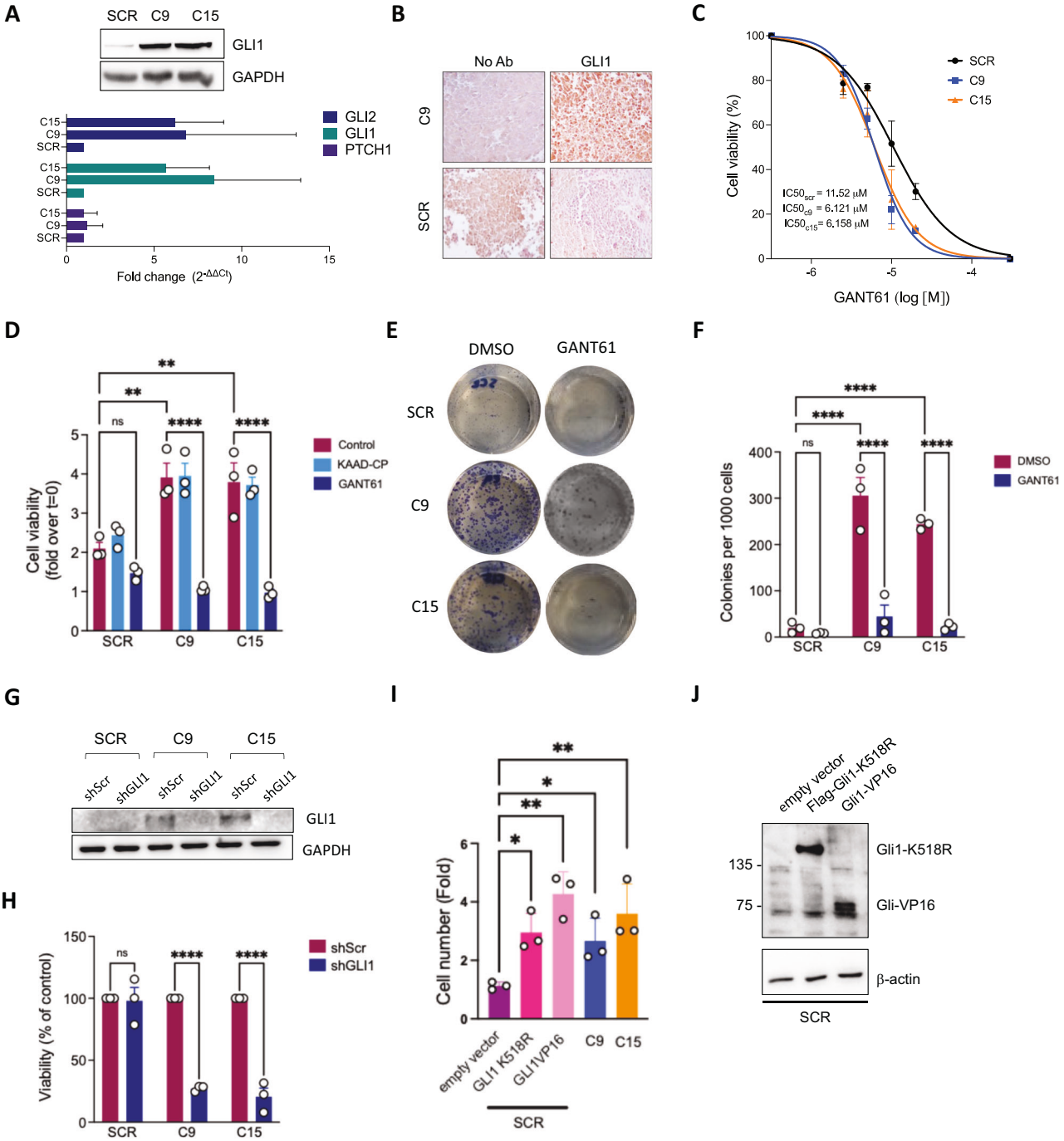

Fig. 2 PTCH1 CTD truncation leads to non-canonical upregulation of GLI transcription factors. A Top: GLI1 protein levels in SCR, C9 and C15 cells. GAPDH is shown as loading control. Bottom: expression of *PTCH1*, *GLI1* and *GLI2* by qPCR. Expression levels were normalized to *GAPDH* mRNA and represented as fold change relative to control SCR cells ($n = 3$). **B** Representative images for IHC staining of GLI1 and negative control (NoAb- no primary antibody) in sections of xenograft tumours generated with SCR and C9 cells. **C** Effect of increasing concentrations of GANT61 on viability of SCR, C9 and C15 cells after 72 h ($n = 3$). The inset displays the calculated IC_{50} in each cell line. **D** Effect of 0.5 μM KAAD-cyclopamine (KAAD-CP), 5 μM GANT61 or vehicle (DMSO) on the viability of SCR, C9 and C15 cells after 72 h ($n = 3$). **E** Effect of 5 μM GANT61 or vehicle control (DMSO) on the colony formation ability of SCR, C9 and C15 cells upon culture for 10 days (representative images at the end of the experiment). **F** Number of colonies per 1000 plated cells at day 10 in the same conditions as (**E**) ($n = 3$). **G** GLI1 protein levels in SCR, C9 and C15 cells transduced with lentiviruses encoding control scrambled (shScr) or GLI1 targeting (shGLI1) shRNAs. **H** Viability of SCR, C9 and C15 cells following 72 h of transduction with shScr-lenti or shGLI1-lenti in complete medium. Data are expressed as % of shScr ($n = 3$). **I** Change in cell number of SCR cells in complete medium 48 h after transfection with empty vector, Gli1 K512R or Gli1(2-413)-VP16, compared to untransfected C9 and C15 cells ($n = 3$). **J** Representative immunoblot depicting Gli1 protein levels following ectopic expression of Flag–Gli1-K518R and/or Gli1(2-413)–VP16 in SCR cells used in the proliferation assay shown in (**I**). The top blot was developed with a mix of anti-Gli1 and anti-VP16 antibodies. β-actin was used as loading control. All quantitative data represent the mean ± SEM of independent biological repeats (indicated n), performed in technical replicates. ns not significant; $^{*}P < 0.05$; $^{**}P < 0.01$; $^{***}P < 0.001$; $^{****}P < 0.0001$.

(Fig. 4G), supporting the notion that transcriptomic changes in cAMP signalling pathways promote proliferation of PTCH1 CTD mutant cells.

PTCH1 CTD truncation leads to upregulation of the EGFR signalling pathway

Consistent with the RNA-seq data, qRT-PCR confirmed the mRNA a ~9 -fold and ~6 -fold upregulation of *EGFR* in C9 and C15 compared to SCR, and of its ligands *AREG* (~16-fold and ~14-fold) and *EREG* (~11 -fold and ~11-fold), respectively (Fig. 5A, top). EREG and AREG are commonly overexpressed in CRC at the transcriptional and protein levels and have been proposed as predictors of response to anti-EGFR therapy in RAS WT CRC [21–23]. Their levels were not significantly reduced by the GLI1/2 inhibitor GANT61 (Fig. S6), suggesting that they are not a consequence of non-canonical activation of GLI transcription. The upregulation of *EGFR*, *AREG* and *EREG* mRNA was maintained in explanted xenografts from C9 cells compared to SCR cells (Fig. 5A, bottom). C9 and C15 cells had increased basal ERK1/2 and Akt phosphorylation level compared SCR cells under serum starvation conditions (Fig. 5B). The EGFR inhibitor erlotinib did not affect cell proliferation of C9 and C15, unlike of SCR cells (Fig. 5C). In addition, erlotinib reduced plating efficiency in colony formation assays in C9 and C15 clones by 61% and 55%, respectively; however, the PTCH1 CTD mutant clones still formed more colonies than the PTCH1 WT cells (Fig. 5D). The partial effect of erlotinib on SCR cells is not surprising since SW620 is a *KRAS* mutated cell line, and thus upstream activation of EGFR signalling is expected to have only a partial effect on signalling downstream of RAS. To confirm this observation, we treated the cells with cetuximab, a blocking anti-EGFR antibody. Like erlotinib, cetuximab treatment failed to reduce proliferation of SCR, C9 and C15 cells (Fig. 5E). Instead, inhibition of MEK with trametinib reduced ERK1/2 phosphorylation (Fig. 5F) and proliferation of SCR, C9 and C15 cells in a dose dependent manner (Figs. 5G and S7). A second MEK inhibitor, UO126, also showed a strong antiproliferative effect in all groups (Fig. S7). Therefore, PTCH1 CTD mutant cells do not show a higher sensitivity to MEK inhibitors, suggesting that additional mechanisms support their proliferative advantage.

Increased tumourigenesis of PTCH1 CTD truncated cells is dependent on hyperactivation of PI3K

Next, we tested the role of PI3K/Akt signalling in the enhanced proliferation of C9 and C15 cells. A low concentration of the PI3K

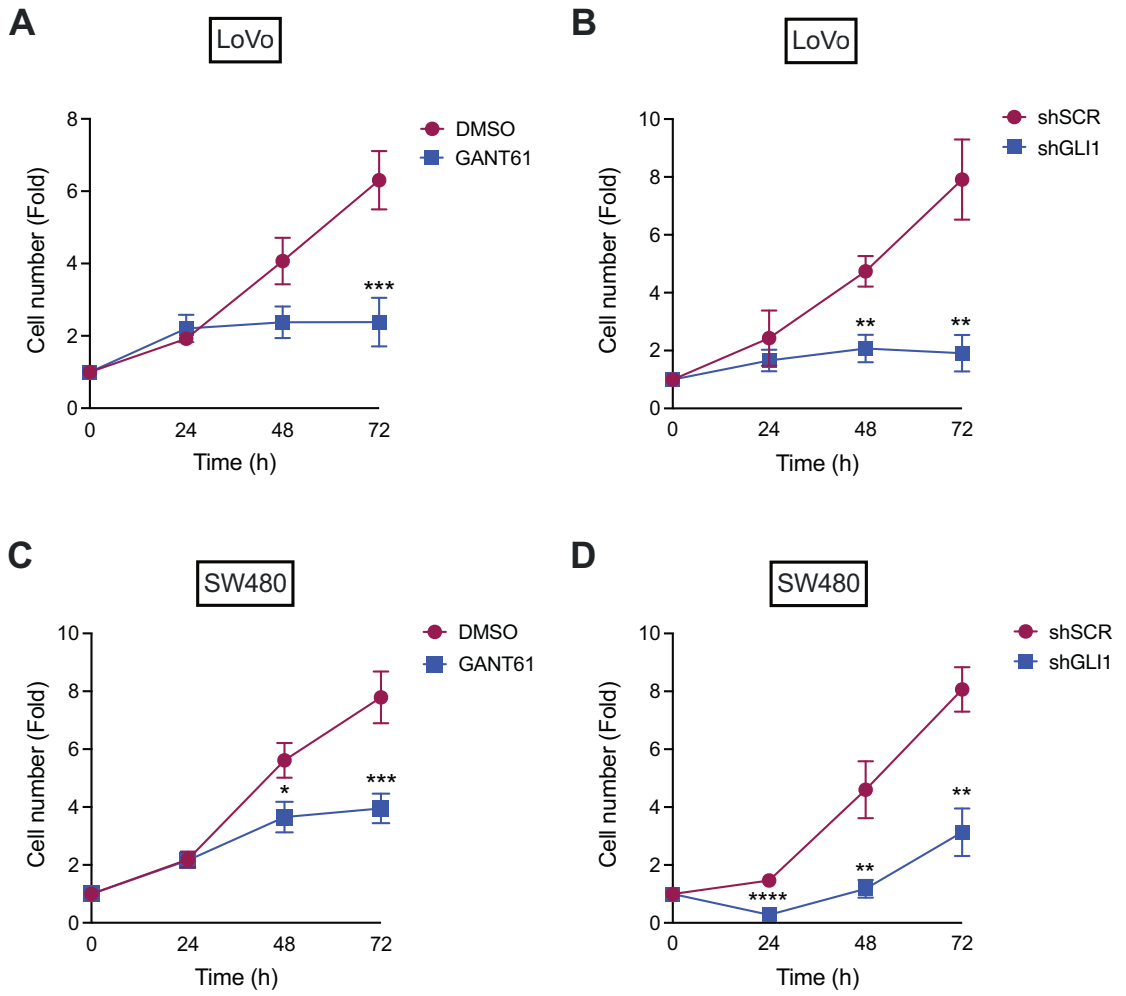

Fig. 3 Colorectal cancer cells with natural PTCH1 CTD indels are dependent on GLI1. A Change in LoVo cell number over time cultured in the presence of DMSO (control) or 5 μM GANT61 ($n = 3$). **B** Change in LoVo cell number over time following transduction with shScr-lenti or shGLI1-lenti ($n = 3$). **C** Change in SW480 cell number over time cultured in the presence of DMSO (control) or 5 μM GANT61 ($n = 3$). **D** Change in SW480 cell number over time following transduction with shScr-lenti or shGLI1-lenti ($n = 3$). All quantitative data represent the mean ± SEM of independent biological repeats (indicated n), performed in technical replicates. *$P < 0.05$; **$P < 0.01$; ***$P < 0.001$; ****$P < 0.0001$.

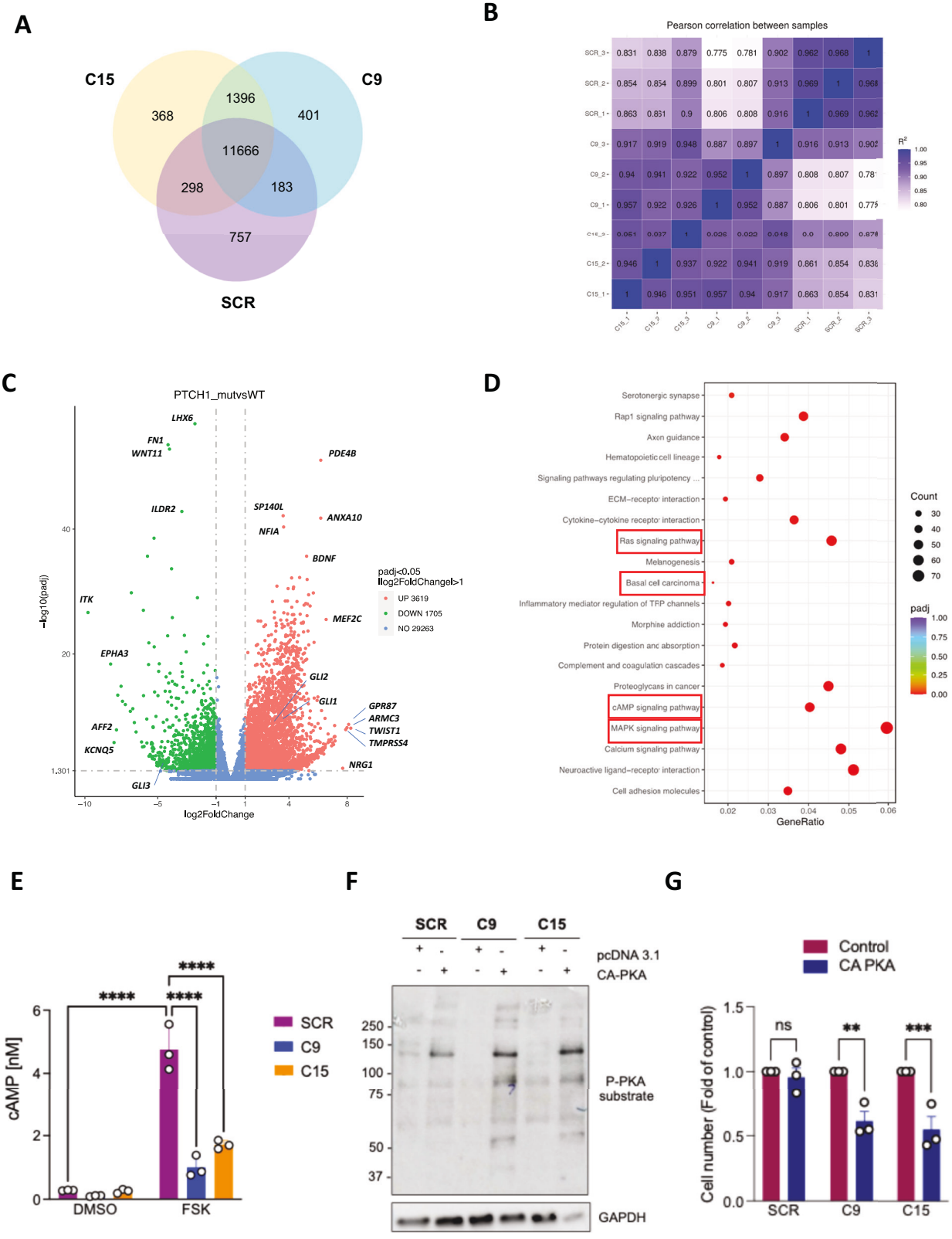
A
C15
C9
SCR
368
1396
401
11666
298
183
757
B
Pearson correlation between samples
C
PTCH1_mutvsWT
padj<0.05
|log2FoldChange|>1
UP 3619
DOWN 1705
NO 29263
−log10(padj)
log2FoldChange
LHX6
FN1
WNT11
PDE4B
ILDR2
SP140L
ANXA10
NFIA
BDNF
ITK
MEF2C
EPHA3
GLI2
GLI1
GPR87
ARMC3
TWIST1
TMPRSS4
AFF2
KCNQ5
NRG1
GLI3
D
Serotonergic synapse
Rap1 signaling pathway
Axon guidance
Hematopoietic cell lineage
Signaling pathways regulating pluripotency ...
ECM−receptor interaction
Cytokine−cytokine receptor interaction
Ras signaling pathway
Melanogenesis
Basal cell carcinoma
Inflammatory mediator regulation of TRP channels
Morphine addiction
Protein digestion and absorption
Complement and coagulation cascades
Proteoglycans in cancer
cAMP signaling pathway
MAPK signaling pathway
Calcium signaling pathway
Neuroactive ligand−receptor interaction
Cell adhesion molecules
GeneRatio
Count
padj
E
cAMP [nM]
DMSO
FSK
SCR
C9
C15
F
SCR
C9
C15
pcDNA 3.1
CA-PKA
P-PKA substrate
GAPDH
G
Control
CA PKA
Cell number (Fold of control)
ns
SCR
C9
C15

Fig. 4 PTCH1 CTD mutant clones have transcriptional upregulation of cancer-related pathways. A Venn diagram showing gene co-expression among SCR, C9 and C15 clones ($n = 3$ biological repeats). **B** Pearson correlation of gene count reads between each biological repeat of the SCR, C9, C15 groups. **C** Volcano plot of statistically significantly expressed genes (-log10(Padj)>1.301) between both C9 and C15 clones ("PTCH1 mut") and SCR cells ("WT"). **D** Most upregulated pathways in PTCH1 mut vs. WT cells by KEEG analysis. The size of the dot represents the gene count in that category and the colour reflects the Padj value. **E** cAMP production in basal conditions (growth medium supplemented with DMSO) or after 10 min stimulation with 3 μM forskolin (FSK) in SCR, C9 and C15 cells ($n = 3$). **F** Representative immunoblot of phosphorylated-PKA substrates in SCR, C9 and C15 cells 48 h after transfection with empty vector (pcDNA3.1) or a plasmid encoding a constitutively active PKA (CA-PKA). GAPDH was used as a loading control. **G** Change in cell number of SCR, C9 and C15 48 h after transfection with empty vector (control) or a plasmid encoding a constitutively active PKA (CA-PKA) ($n = 3$). All quantitative data represent the mean ± SEM of independent biological repeats (indicated n), performed in technical replicates. ns not significant; $^{**}P < 0.01$; $^{****}P < 0.0001$.

inhibitor BKM-120 (buparlisib) decreased P-Akt (Fig. 6A) and specifically reduced the proliferation rate of both PTCH1 CTD mutant clones without affecting proliferation of isogenic cells expressing WT PTCH1 (Fig. 6B). BKM-120 IC_{50} was lower in C9 and C15 clones compared to SCR cells, in agreement with their increased sensitivity to low concentrations (Fig. 6C). Colony formation was also reduced dose-dependently by BKM-120 in PTCH1 mutant clones (Fig. 6D, E). Given the central role of GLI1 in the proliferative advantage of PTCH1 CTD mutant cells, we investigated if normalisation of the cell's behaviour by PI3K inhibition was mediated by changes in GLI1. BKM-120 treatment reduced *GLI1* mRNA levels (Fig. 6F), suggesting that PI3K signalling is partly required for upregulation of GLI1 downstream of the PTCH1 CTD mutation. A second PI3K inhibitor, LY294002, also caused a reduction in GLI1 expression (Fig. S8). We have previously reported that GLI activation requires PI3K signalling through Akt, and that the latter opposes PKA-mediated phosphorylation and degradation of GLI2 [24]. Therefore, we tested whether a dominant negative Akt1 mutant (Akt1 S473A/T308A) could mimic the effect of PI3K inhibition. Transfection of SCR, C9 and C15 cells with dnAkt specifically abolished the enhanced proliferation of C9 and C15 cells (Fig. 6G). Interestingly, lysates of cells with lentiviral-mediated knockdown of GLI1 from Fig. 2 showed a strongly reduced P-Akt signal and, to a lower extent, P-ERK1/2 levels (Fig. 6H), suggesting that sustained PI3K/Akt activation in PTCH1 CTD mutant cells is also propelled by GLI1, leading to a positive feedback loop (Fig. 6I). Notwithstanding, increasing Akt signalling by expression of a constitutively active Akt1 mutant (myr-Akt1) was insufficient to rescue proliferation in cells treated with the Gli1/2 inhibitor GANT61 (Fig. S9). These observations indicate that the increased tumourigenic capacity of PTCH1 CTD truncated cells is reliant on increased GLI1 expression and activity, which is maintained by hyperactivation of PI3K/Akt pathway.

DISCUSSION

The canonical Hedgehog (Hh) signalling pathway, driving activation of SMO and GLI1, underlies tumourigenesis of basal cell carcinoma and Shh-type medulloblastoma; however, its role in CRC and other cancers of epithelial origin remains controversial. While CRC patients with increased expression of *GLI1* have decreased overall survival [25], the pharmacological SMO inhibitor vismodegib did not show additional benefits to standard treatment in patients with metastatic colon cancer [24]. Here, we link frameshift mutations in the *PTCH1* gene that result in early truncation of the PTCH1 CTD in CRC with SMO-independent upregulation of GLI1. In this study, we show that CRC cells engineered to endogenously express PTCH1 with a truncated CTD, found in ~4% of CRC patients, are characterized by increased proliferation, reduced apoptosis and increased anchorage-independent growth in vitro and form larger tumours in vivo compared to isogenic cells expressing WT PTCH1. PTCH1 CTD mutant cells show non-canonical upregulation of GLI1, which was surprising as the resulting truncations in the PTCH1 CTD did not impair SMO control. GLI1 upregulation is a hallmark of increased transcriptional activity of the GLI transcription factor family. The other family members, GLI2 and GLI3, are constitutively expressed and activated in response to diverse stimuli, mainly by Hh binding to PTCH1 leading to SMO activation, but also by crosstalk with other pathways in a SMO-independent manner. When GLI2 and GLI3 are activated, they induce GLI1 expression by binding to GLI-responsive elements in its promoter. Phosphorylation of GLI1 and GLI2 by PKA triggers additional post-translational modifications that mark them for proteasomal degradation, while phosphorylation of GLI3 leads to partial processing into a transcriptional repressor [1, 26]. We propose that the reduced cAMP concentrations and lower PKA activity observed in PTCH1 CTD mutant cells contributes to the increased GLI activity.

We have previously shown that GLI transcriptional activity is stimulated by crosstalk with the MAPK and PI3K signalling pathways [26, 27]. RNA-seq revealed vast transcriptome changes due to premature truncation of PTCH1, which pointed towards increased MAPK and PI3K/Akt signalling, confirmed at the protein level as increased ERK1/2 and Akt phosphorylation, despite all cells being *KRAS* mutated. However, our results indicate that the growth advantage of the PTCH1 mutant cells is primarily driven by increased PI3K/Akt signalling, acting through increasing GLI1 activity and expression. This feature explains the insensitivity to KAAD-cyclopamine that we observed and predicts lack of response to vismodegib and other FDA-approved SMO inhibitors, as previously reported [28]. Moreover, the findings suggest a potential vulnerability of PTCH1 CTD mutant CRC cases to buparlisib or other PI3K inhibitors.

The results also showed that GLI1 upregulation is essential for maintaining the more aggressive phenotype of PTCH1 CTD mutant cancer cells in vitro and in vivo. Unlike approaches that target SMO, inhibition or silencing of GLI effectively blocked proliferation and colony formation capacity of PTCH1 CTD truncated CRC cells. Moreover, blocking GLI1 strongly impaired doubling of LoVo and SW480 CRC cell lines, in which the PTCH1 CTD mutations are naturally occurring. Interestingly, inhibition or silencing of GLI1 also reduced P-Akt levels in PTCH1 CTD mutant cells. Together with the loss of proliferative advantage in PTCH1 CTD mutant cells by PI3K inhibition, we propose that upregulation of GLI1 increased oncogenic properties in these cells through activation of a GLI1/PI3K positive signalling loop.

PTCH1 CTD mutations are much more prevalent, if not exclusive, in colon cancers derived from the ascending and transversal colon, characterised by higher incidence of *BRAF* mutations and lower incidence of *KRAS* mutations than left-sided colon cancers. Amongst the most upregulated genes in PTCH1 CTD mutant cells were *EREG* and *AREG*, which are predictive biomarkers for anti-EGFR therapy responsiveness in *RAS* WT CRC patients [22, 23, 28]. However, upregulation of *EGFR*, *AREG* and *EREG* in cells carrying CTD-truncated PTCH1 did not translate into increased sensitivity to the EGFR inhibitors erlotinib and cetuximab nor to the MEK inhibitors trametinib and UO126, likely due to a compensatory increase in survival through activation of the PI3K-GLI1 loop. This suggests that the *PTCH1* mutational status could be a predictor of responsiveness

Table 1. Selected upregulated genes in C9 and C15 cells compared to SCR cells.

Gene symbol	Gene name	Log2Fold	Padjust
Hedgehog signalling pathway			
HHIP	Hedgehog interacting protein	3.59	0.0031
PTCH2	Patched 2	1.77	9.37×10^{-5}
DISP1	Dispatched RND transporter family member 1	1.76	2.32×10^{-7}
GLI1	GLI family zinc finger 1	3.43	1.39×10^{-8}
GLI2	GLI family zinc finger 2	3.10	1.38×10^{-8}
MOSMO	Modulator of smoothened	1.33	1.99×10^{-5}
HHAT	Hedgehog acyltransferase	3.83	3.25×10^{-12}
EGFR signalling pathway			
EGFR	Epidermal growth factor receptor	3.94	1.05×10^{-18}
AREG	Amphiregulin	4.37	6.65×10^{-8}
EREG	Epiregulin	3.83	9.15×10^{-15}
NRG1	Neuregulin	7.69	0.02
EGF	Epidermal growth factor	4.13	0.018
BTC	Betacellulin	3.26	3.31×10^{-12}
Ras signalling pathway			
RASGRP2	RAS guanyl releasing protein 2	3.83	6.75×10^{-22}
RASSF2	Ras association domain family member 2	3.35	1.23×10^{-17}
RASD2	RASD family member 2	3.06	2.35×10^{-12}
MRAS	muscle RAS oncogene homolog	2.99	5.81×10^{-13}
RRAS	RAS related	2.72	9.39×10^{-9}
RASGEF1A	RasGEF domain family member 1A	2.58	3.05×10^{-12}
RASGEF1C	RasGEF domain family member 1C	2.55	9.14×10^{-5}
RASGRP3	RAS guanyl releasing protein 3	2.53	0.0033
RASGRP4	RAS guanyl releasing protein 4	2.14	0.0030
RASGRP1	RAS guanyl releasing protein 1	1.95	5.75×10^{-5}
GAB1	GRB2 associated binding protein 1	1.96	5.08×10^{-6}
GAREM2	GRB2 associated regulator of MAPK1 subtype 2	1.71	
GAREM1	GRB2 associated regulator of MAPK1 subtype 1	1.28	2.88×10^{-6}
GAB3	GRB2 associated binding protein 3	5.10	0.0016
TGFβ signalling pathway			
SMAD3	SMAD family member 3	1.49	4.96×10^{-7}
SMAD2	SMAD family member 2	1.05	4.46×10^{-6}
SMAD4	SMAD family member 4	3.87	2.28×10^{-22}
PKA signalling pathway			
PRKAR2B	Protein kinase cAMP-dependent type II regulatory subunit beta	3.68	6.73×10^{-12}
PRKACB	Protein kinase cAMP-activated catalytic subunit beta	2.21	9.55×10^{-19}
AKAP3	A-kinase anchoring protein 3	2.24	1.18×10^{-6}
AKAP11	A-kinase anchoring protein 11	1.11	1.26×10^{-5}
AKAP12	A-kinase anchoring protein 12	3.83	4.27×10^{-17}
PDE4C	Phosphodiesterase 4C	3.72	0.044
PDE9A	Phosphodiesterase 9A	1.63	8.59×10^{-6}
PDE5A	Phosphodiesterase 5A	1.19	0.0052
PDE4A	Phosphodiesterase 4A	1.10	5.57×10^{-6}
PDE4B	Phosphodiesterase 4B	6.18	9.41×10^{-52}
PDE7B	Phosphodiesterase 7B	5.82	0.00011
PDE10A	Phosphodiesterase 10A	4.58	0.0094
PDE6A	Phosphodiesterase 6A	4.35	0.0175
PDE1C	Phosphodiesterase 1C	4.27	0.021
PDE2A	Phosphodiesterase 2A	4.18	1.09×10^{-6}

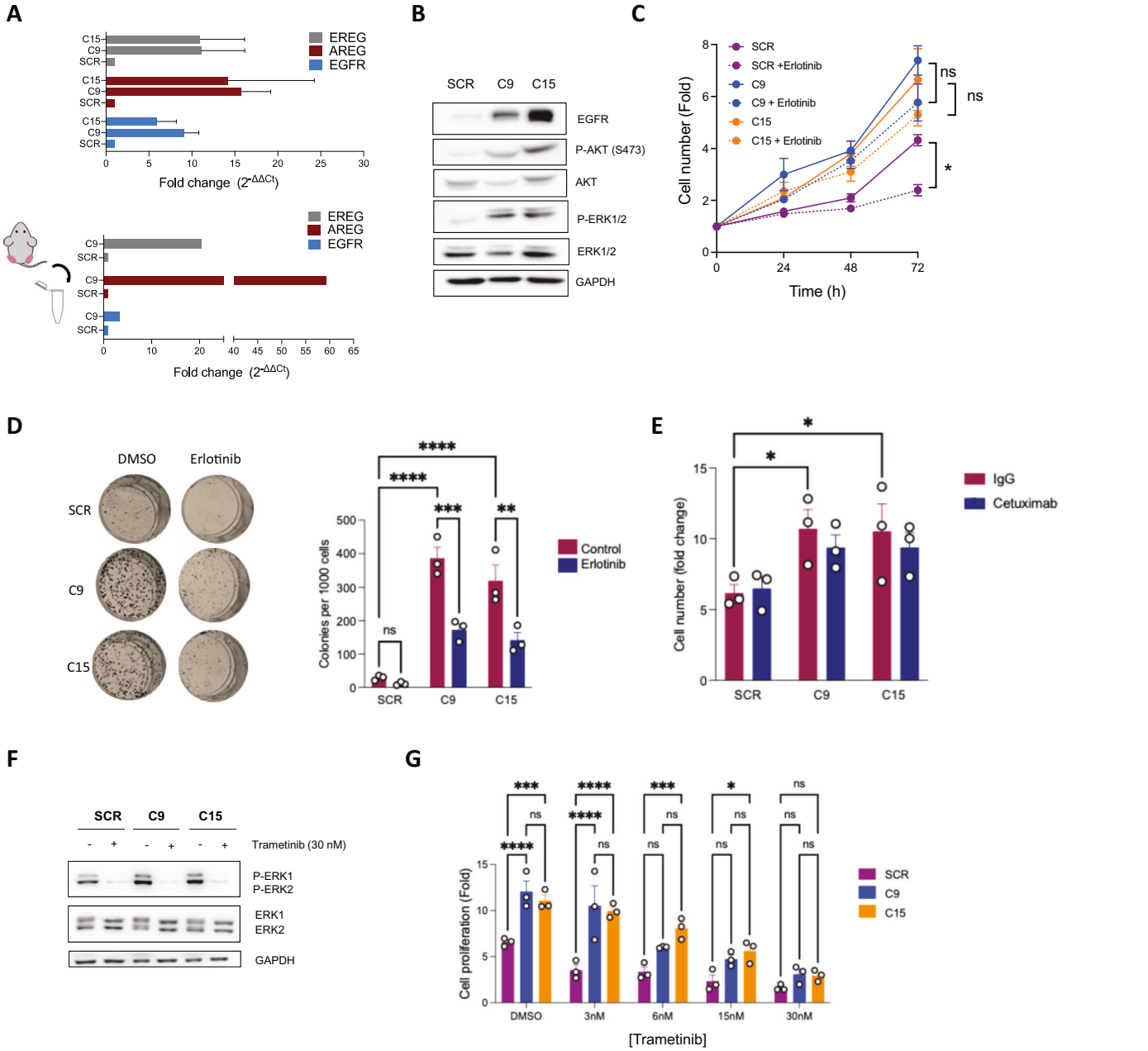

Fig. 5 Upregulation of EGFR-MAPK signalling in PTCH1 CTD mutant cells. A Top: *EREG*, *AREG*, and *EGFR* mRNA expression in SCR, C9, and C15 cells by qPCR. Expression levels were normalized to *GAPDH* mRNA and represented as fold change relative to control SCR cells ($n = 3$). Bottom: expression of the same genes in pooled RNA from xenografts derived from SCR and C9 cells. **B** Representative western blot of EGFR, phospho-Akt, phospho-ERK1/2, total Akt, total ERK1/2, and GADPH in SCR, C9, and C15 cells. **C** Effect of 10 μM Erlotinib or vehicle control on cell proliferation of SCR, C9 and C15 cells over time ($n = 3$). **D**. Effect of 10 μM Erlotinib or vehicle control (DMSO) on the colony formation ability of SCR, C9 and C15 cells upon culture for 10 days. Left: representative images at the end of the experiment. Right: number of colonies per 1,000 plated cells at day 10 ($n = 3$). **E** Effect of 10 μg/ml Cetuximab or a control IgG on the cell number of SCR, C9 and C15 cells after 72 h treatment ($n = 3$). **F** Effect of 30 nM Trametinib or DMSO vehicle on phospho-ERK1/2 levels in SCR, C9 and C15 cells. **G** Dose dependent reduction of cell proliferation in SCR, C9, and C15 cells treated with Trametinib for 72 h ($n = 3$). All quantitative data represent the mean ± SEM of independent biological repeats (indicated n), performed in technical replicates. ns = not significant; *$P < 0.05$; **$P < 0.01$; ***$P < 0.001$; ****$P < 0.0001$.

to anti-EGFR therapy and anti-PI3K/Akt therapeutics. Therefore, we propose that *PTCH1* sequencing could be beneficial for stratification of patients with right-sided colon cancer to guide the choice of better targeted therapeutic interventions.

In conclusion, this study supports a pathogenic role of frameshift mutations in exons 22-23 of *PTCH1*, encoding the CTD. Our data provide mechanistic insights of the effect of *PTCH1* mutations in CRC and identify therapeutic vulnerabilities.

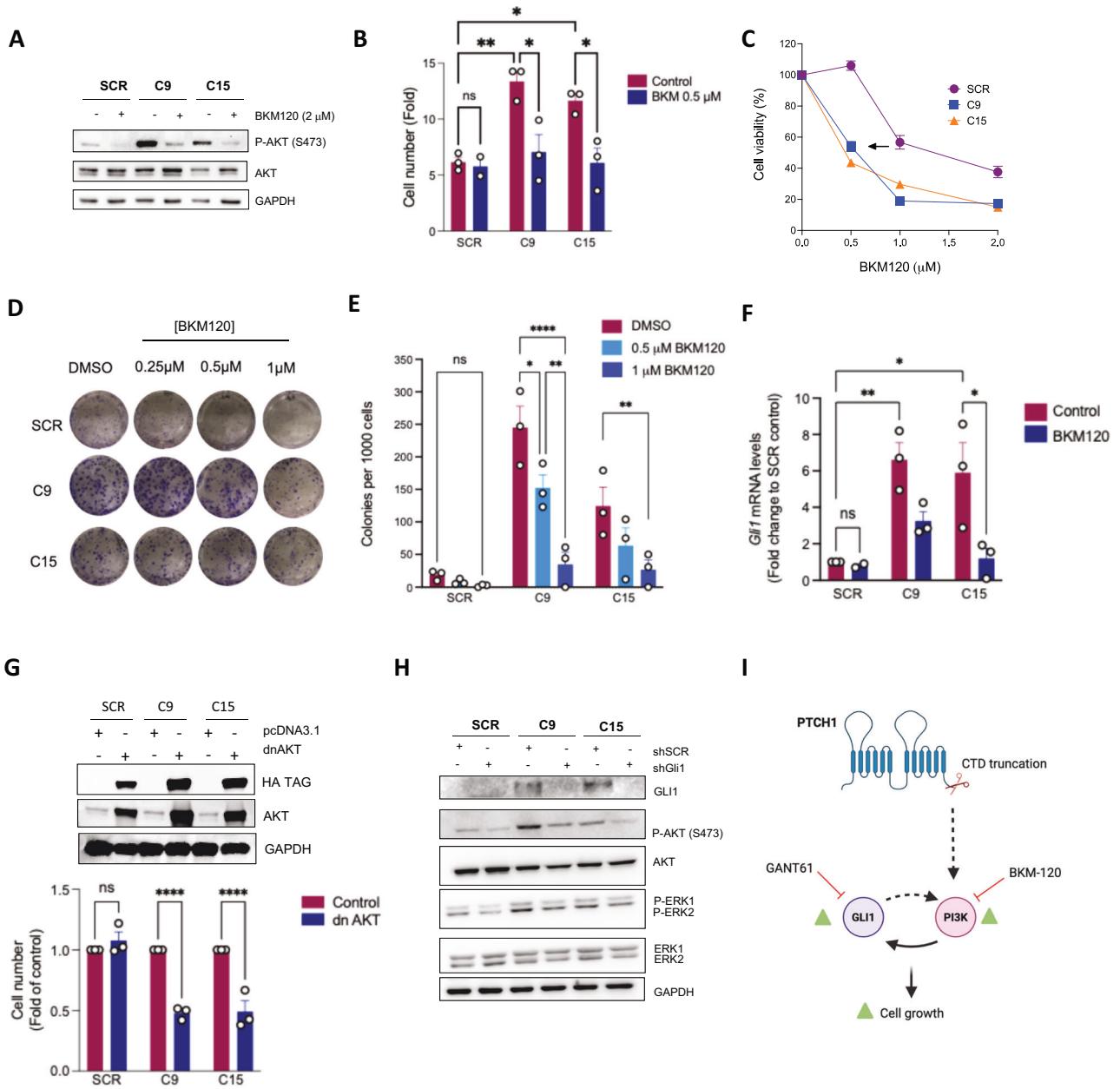

Fig. 6 A positive PI3K/Akt-GLI loop in PTCH1 mutant cells underlies their growth advantage. A Effect of 2 μM BKM-120 or DMSO vehicle on phospho-Akt(S473) and total Akt levels in SCR, C9 and C15 cells. GAPDH was used as a loading control. **B** Effect of 0.5 μM BKM-120 or DMSO (control) on cell number of SCR, C9 and C15 at 72 h ($n = 3$). **C** Reduction of viability in SCR, C9, and C15 cells treated with increasing concentrations of BKM-120 for 72 h (n = 3). **D** Effect of 0.25, 0.5 and 1 μM BKM-120 or vehicle control (DMSO) on the colony formation ability of SCR, C9 and C15 cells upon culture for 10 days (representative images at the end of the experiment). **E** Quantification of number of colonies formed per 1,000 plated SCR, C9 and C15 cells treated with DMSO or 0.5-1 μM BKM120 for 10 days ($n = 3$). **F** Effect of 0.5 μM BKM-120 or vehicle control on *GLI1* mRNA levels in SCR, C9 and C15 cells by qPCR. Values are normalised to *GAPDH* expression and represent the ΔΔCt ($n = 3$). **G** Top: Representative immunoblot of dominant negative Akt (HA-tag) and total Akt (endogenous plus transfected) in SCR, C9 and C15 cells 48 h after transfection with empty vector (pcDNA3,1) or dnAkt (S473A/T308A) (dnAkt). Bottom: Change in cell number of SCR, C9 and C15 48 h after transfection with empty vector (control) or a plasmid encoding dnAkt ($n = 3$). **H** Protein levels of GLI1, phospho-Akt, total Akt, phospho-ERK1/2, total ERK1/2 and GAPDH in SCR, C9 and C15 cells transduced with lentiviruses encoding control scrambled (shScr) or GLI1 targeting (shGLI1) shRNA. **I** Proposed model of a positive feedback loop between GLI1 and PI3K triggered by PTCH1 CTD truncations. Dotted lines indicate potentially indirect mechanisms. All quantitative data represent the mean ± SEM of independent biological repeats (indicated n), performed in technical replicates. ns = not significant; *$P < 0.05$; **$P < 0.01$; ***$P < 0.001$; ****P < 0.0001.

DATA AVAILABILITY

The raw fastp sequencing files and the total read counts related to the RNA-seq data presented in this manuscript can be accessed at the Gene Expression Omnibus using accession number GSE293576.

REFERENCES

1. Zhang Y, Beachy PA. Cellular and molecular mechanisms of Hedgehog signalling. Nat Rev Mol Cell Biol. 2023;24:668–687.
2. Ingham PW. Hedgehog signaling. Curr Top Dev Biol. 2022;149:1–58.
3. Jing J, Wu Z, Wang J, Luo G, Lin H, Fan Y, et al. Hedgehog signalling in tissue homoeostasis, cancers, and targeted therapies. Signal Transduct Target Ther. 2023;8:315.
4. Thibert C, Teillet MA, Lapointe F, Mazelin L, Le Dourain NM, Mehlen P. Inhibition of neuroepithelial patched-induced apoptosis by sonic hedgehog. Science. 2003;301:843–846.
5. Chen X, Morales-Alcala CC, Riobo-Del Galdo NA. Autophagic flux is regulated by interaction between the C-terminal domain of PATCHED1 and ATG101. Mol Cancer Res. 2018;16:909–919.
6. Brennan D, Chen X, Cheng L, Mahoney M, Riobo NA. Noncanonical Hedgehog Signaling. Vit Horm. 2012;88:55–72.
7. Mille F, Thibert C, Fombonne J, Rama N, Guix C, Hayashi H, et al. The Patched dependence receptor triggers apoptosis through a DRAL-caspase 9 complex. Nat Cell Biol. 2009;11:739–746.
8. Chen XL, Chinchilla P, Fombonne J, Ho L, Guix C, Keen JH, et al. Patched-1 proapoptotic activity is downregulated by modification of K1413 by the E3 ubiquitin-protein ligase Itchy homolog. Mol Cell Biol. 2014;34:3855–3866.
9. Kim J, Hsia EY, Brigui A, Plessis A, Beachy PA, Zheng X. The role of ciliary trafficking in Hedgehog receptor signaling. Sci Signal. 2015;8:ra55.
10. Fleet A, Lee JP, Tamachi A, Javeed I, Hamel PA. Activities of the cytoplasmic domains of patched-1 modulate but are not essential for the regulation of canonical hedgehog signalling. J Biol Chem. 2016;291:17557–17568.
11. Toftgard R. Hedgehog signalling in cancer. Cell Mol Life Sci. 2000;57:1720–1731.
12. Watkins DN, Berman DM, Burkholder SG, Wang B, Beachy PA, Baylin SB. Hedgehog signalling within airway epithelial progenitors and in small-cell lung cancer. Nature. 2003;422:313–317.
13. Berman DM, Karhadkar SS, Maitra A, Montes de Oca R, Gerstenblith MR, Briggs K, et al. Widespread requirement for Hedgehog ligand stimulation in growth of digestive tract tumours. Nature. 2003;425:846–851.
14. Thayer SP, Pasca di Magliano M, Heiser PW, Nielsen CM, Roberts DJ, Lauwers GY, et al. Hedgehog is an early and late mediator of pancreatic cancer tumorigenesis. Nature. 2003;425:851–856.
15. Pietrobono S, Gagliardi S, Stecca B. Non-canonical hedgehog signaling pathway in cancer: Activation of GLI transcription factors beyond smoothened. Front Genet. 2019;10:556.
16. Caballero-Ruiz B, Gkotsi DS, Ollerton H, Morales-Alcala CC, Bordone R, Jenkins GML, et al. Partial Truncation of the C-Terminal Domain of PTCH1 in Cancer Enhances Autophagy and Metabolic Adaptability. Cancers. 2023;15:369.
17. Borowicz S, Van Scoyk M, Avarasala S, Rathinam MKK, Tauler J, Bikkavilli RK, et al. The soft agar colony formation assay. J Vis Exp. 2014;92:e51998.
18. Canettieri G, Di Marcotullio L, Greco A, Coni S, Antonucci L, Infante P, et al. Histone deacetylase and Cullin3-REN^{KCTD11} ubiquitin ligase interplay regulates Hedgehog signalling through Gli acetylation. Nat Cell Biol. 2010;12:132–142.
19. Barczak W, Sucharska W, Rubis B, Kulcenty K. Universal Real-Time PCR-Based Assay for Lentiviral Titration. Mol Biotechnol. 2015;57:195–200.
20. Berg KCG, Eide PW, Eilertsen IA, Johannessen B, Bruun J, Danielsen SA, et al. Multi-omics of 34 colorectal cancer cell lines – a resource for biomedical studies. Mol Cancer. 2017;16:116.
21. Wasson CW, Caballero-Ruiz B, Gillespie J, Derret-Smith E, Mankouri J, Denton CO, et al. Induction of pro-fibrotic CLIC4 in dermal fibroblasts by TGF-b/Wnt3a is mediated by GLI2 upregulation. Cells. 2022;11:530.
22. Khambata-Ford S, Garret CR, Meropol NJ, Basik M, Harbison CT, Wu S, et al. Expression of epiregulin and amphiregulin and K-ras mutation status predict disease control in metastatic colorectal cancer patients treated with cetuximab. J Clin Oncol. 2007;25:3230–3237.
23. Jing C, Jin YH, You Z, Qiong Q, Jun Z. Prognostic value of amphiregulin and epiregulin mRNA expression in metastatic colorectal cancer patients. Oncotarget. 2016;7:55890–55899.
24. Berlin J, Bendell JC, Hart LL, Firdaus I, Gore I, Hermann RC, et al. A randomized phase II trial of vismodegib versus placebo with FOLFOX or FOLFIRI and bevacizumab in patients with previously untreated metastatic colorectal cancer. Clin Cancer Res. 2013;19:258–267.
25. Magistri P, Battistelli C, Strippoli R, Petrucciani N, Pellinen T, Rossi L, et al. SMO inhibition modulates cellular plasticity and invasiveness in colorectal cancer. Front Pharmacol. 2018;8:956.
26. Riobo NA, Lu K, Ai X, Haines GM, Emerson CP Jr. Phosphoinositide 3-kinase and Akt are essential for Sonic Hedgehog signaling. Proc Natl Acad Sci USA. 2006;103:4505–4510.
27. Riobo NA, Haines GM, Emerson CP Jr. Protein kinase C-delta and mitogen-activated protein/extracellular signal regulated kinase-1 control GLI activation in hedgehog signaling. Cancer Res. 2006;66:839–845.
28. Seligmann JF, Elliot F, Richman SD, Jacobs B, Hemmings G, Brown S, et al. Combined Epiregulin and Amphiregulin expression levels as a predictive biomarker for panitumumab therapy benefit or lack of benefit in patients with RAS wild-type advanced colorectal cancer. JAMA Oncol. 2016;2:633–642.

ACKNOWLEDGEMENTS

We thank Devon Ivy (University of Rome) for technical support with tissue sectioning and Andrew Macdonald (University of Leeds) for P-PKA substrate antibody. This study was funded by the BBSRC grants BB/S01716X/1 and BB/W018640/1 to NARDG; Sapienza University of Rome doctoral fellowship to BCR; AIRC IG 25833, MUR PRIN 2022 2022L332YR, MUR PRIN PNRR P202243FBL to GC; MUR PRIN 2022 under 40 2022J8X7PJ to SC; AIRC Italy Post-Doc fellowship 29605 to RB.

AUTHOR CONTRIBUTIONS

Cell experiments: BCR, RB and EG; animal experiments: BCR and SC; immunostaining: BCR and SC; bioinformatic analysis: DSG; cell data analysis: BCR; conceptualisation: GC and NARDG; manuscript draft: BCR and NARDG; manuscript review and editing: GC and NARDG; funding acquisition: GC and NARDG.

COMPETING INTERESTS

The authors declare no competing interests.

ADDITIONAL INFORMATION

Supplementary information The online version contains supplementary material available at https://doi.org/10.1038/s41388-026-03698-9.

Correspondence and requests for materials should be addressed to Gianluca Canettieri or Natalia A. Riobo-Del Galdo.